Chapter 7
Magneto-Nanosensor Diagnostic Chips

Richard S. Gaster, Drew A. Hall, and Shan X. Wang

Abstract We have developed an automated assay for disease biomarker detection that can be run on a handheld sensing platform. By coupling magnetic nanotechnology with an array of magnetically responsive nanosensors, we demonstrate a rapid, multiplex immunoassay that eliminates the need for trained technicians to run molecular diagnostic tests. A major limitation for other detection modalities is signal distortion that occurs due to background heterogeneity in ionic strength, pH, temperature, and autofluorescence. Here, we present a magnetic nanosensor technology that is insensitive to background yet still capable of rapid, multiplex protein detection with resolution down to attomolar concentrations and extensive linear dynamic range. The insensitivity of our detector to various media enables our technology to be directly applied to a variety of settings such as molecular biology and clinical diagnostics.

R.S. Gaster
Department of Bioengineering, Medical Scientist Training Program, School of Medicine, Stanford, CA 94305, USA

D.A. Hall
Department of Electrical Engineering, Stanford University, Stanford, CA 94305, USA
e-mail: drewhall@UCSD.EDU

S.X. Wang (✉)
Department of Electrical Engineering, Stanford University, Stanford, CA 94305, USA

Department of Materials Science and Engineering, Stanford University, Stanford, CA 94305, USA
e-mail: sxwang@stanford.edu

D. Issadore and R.M. Westervelt (eds.), *Point-of-Care Diagnostics on a Chip*, Biological and Medical Physics, Biomedical Engineering,
DOI 10.1007/978-3-642-29268-2_7, © Springer-Verlag Berlin Heidelberg 2013

7.1 Introduction

Clinical diagnostics have tremendous potential to revolutionize the practice of medicine. The worldwide research community has made great strides toward developing faster, more sensitive, and more cost-effective diagnostic technologies. Despite extensive progress, however, worldwide access to many revolutionary technologies remains limited to large centralized laboratories in the developed world. Some of the most promising technological advances have combined engineering, material science, chemistry, and physics in the development of devices on the nanoscale, 1–100 nm. The size scale of these devices has been demonstrated to have unique physical and/or chemical properties that can be exploited for biological applications. In addition, the exceptionally small scale enables the detection platform to be highly portable, require relatively low power, and compile numerous sensors into one high-density array for multiplex detection. Accordingly, nanotechnology has been leveraged broadly in both diagnostic medicine and therapeutics.

The diagnosis of a disease requires the identification of a disease marker. The earlier that marker is detected, the earlier the disease can be treated. Typically these disease markers are quantified because ascertaining the concentration aids in determining the prognosis, ideal treatment, or the progression of the disease. Proteins and oligonucleotides, for example, serve as the most common biomolecular markers, termed "biomarkers." Abnormalities in the structure, function, or amount of a biomarker present are what predispose a patient to disease or may be indicative of a particular disease. Because nanosensors are of the same scale as these naturally occurring biomarkers, with nanoscale detection, one can readily interface a highly sensitive sensor with the biological molecule of interest. The use of magnetic nanotechnology for detecting the disease biomarkers holds great promise because magnetically responsive nanosensors often allow for improvement in the lower limit of detection and have the additional advantage of portability of the detection apparatus and ease of use for point-of-care (POC) application. The magnetoresistive biosensors described in this chapter involve three distinct components: the magnetically responsive biosensor itself, the magnetic nanoparticle (MNP) tags, and the protein detection assay. Each aspect will be discussed in detail in this chapter.

7.2 Magnetic Biosensing Modalities

Magnetic biosensing offers several significant advantages over conventional optical techniques and other sensing modalities. The samples (blood, urine, serum, etc.) naturally lack any detectable magnetic content, providing a sensing platform with a very low background. Additionally, MNP tags are not subject to problems that have plagued fluorescent labels such as label bleaching and autofluorescence. Furthermore, the sensors can be arrayed and multiplexed to perform quantitative

protein and/or nucleic acid detection in a single assay without relying on optical scanning. Lastly, the sensors are compatible with standard silicon integrated circuit (IC) technology which allows them to be manufactured with a built-in electronic readout at low cost, in mass quantities, and to be deployed in a one-time use disposable format.

To our knowledge, the first use of MNPs as labels in immunoassays was reported in the literature in 1997 by a group of German researchers [1]. The measurement was achieved by use of a superconducting quantum interference device (SQUID) to detect binding events of magnetically labeled antibodies. While successful, the operating conditions required liquid helium cooling and magnetic shielding, limiting the practicality of the SQUID-based biosensors. In 1998, Baselt first demonstrated detection of MNPs using giant magnetoresistive (GMR) sensors with GMR multilayers [2]. GMR sensors have the advantage of room-temperature operation and simpler instrumentation, making them more attractive, particularly for portable applications.

All magnetoresistive sensors share a common principle of operation where the magnetization of a free magnetic layer (or layers) responds to a change in the local magnetic field and causes a change in the resistance of the sensor. A material that exhibits magnetoresistance transduces a change in an external magnetic field into a change in resistance. This effect was first discovered by Lord Kelvin in 1856 when he found that the resistance of an iron bar increased when the current flowing through the bar was in the same direction as the magnetic field. Furthermore, the resistance decreased when the magnetic field was perpendicular to the current. In actuality, most conductors exhibit magnetoresistance, albeit on an incredibly small scale not useful for transduction. This effect, known as anisotropic magnetoresistance, is commonly used in many sensors today, generally with more efficient materials such as Permalloy ($Ni_{0.2}Fe_{0.8}$). These sensors have typical magnetoresistance (MR) ratios on the order of 2 % at room temperature [3] where the MR ratio is defined as

$$MR = \frac{R_{max} - R_{min}}{R_{min}} = \frac{\Delta R}{R_{min}} \tag{7.1}$$

Many years later came the discovery of GMR which is a quantum mechanical effect wherein a change in magnetic flux is transduced into a change in electrical resistance through spin-dependent scattering. GMR was first observed in a Fe/Cr/Fe thin film stack in 1988 independently by Albert Fert and Peter Grünberg, both of whom went on to win the 2007 Nobel Prize in Physics for their discovery. The most basic device exhibiting this behavior is the multilayer GMR stack where two or more ferromagnetic layers are separated by a thin non-ferromagnetic spacer. The thickness of this non-ferromagnetic spacer is typically only a few nanometers and is critical to the operation of the device. At certain thicknesses, the Ruderman-Kittel-Kasuya-Yosida (RKKY) coupling between the ferromagnetic layers becomes antiferromagnetic, thus causing the magnetization of the adjacent layers to align in an antiparallel state. An external magnetic field rotates the magnetization of the

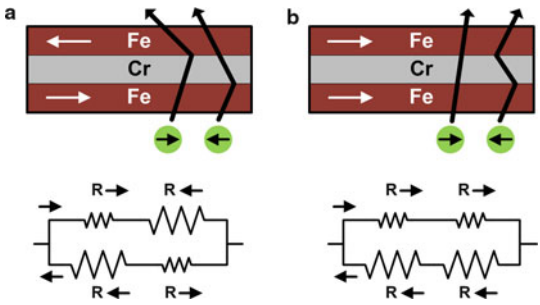

Fig. 7.1 Electrons and corresponding scattering events as they pass through a GMR multilayer film stack with associated circuit model: (**a**) antiparallel state (**b**) parallel state

upper layer causing it to align with the external field, minimizing the total energy of the system.

Qualitatively, the operation of the device can be understood by examining the two extreme cases. In the antiparallel state, as an electron in a spin-up state (designated with an arrow pointing to the right) passes through the film stack, it will scatter when it travels through each ferromagnetic layer (Fig. 7.1a). As it travels through the first ferromagnetic layer, the scattering is relatively small and leads to a low resistance since the spin of the electron is in the same direction as the majority spin of this layer. As the electron continues into the second ferromagnetic layer of the opposite magnetization, it will again scatter. This scattering event, however, is relatively large and leads to a higher resistance because the spin of the electron is in the same direction as the minority spin of this layer. The electron in a spin-down state (designated with an arrow pointing to the left), traveling through a GMR sensor in the antiparallel state, will have a similar resistance to the spin-up electron except in a reversed sequence, where the first layer it travels through is of high resistance and the second layer it travels through is of low resistance. In contrast, in the parallel state, the electron in the spin-up state passes through the first layer and the second layer with relatively few scattering events and thus has a low resistance in its entire path because the spin of the electron is always in the same direction as the majority spin of the layers. The electron in the spin-down state passes through both layers with relatively high resistance because the spin of the electron is always in the same direction as the minority spin of the layers. The overall resistance in each state can be understood using a circuit model where the resistance of the path taken depends on the spin polarization of the electron. For the antiparallel state, each path has a high resistance in series with a low resistance. In the other extreme where a large external magnetic field has caused the two layers to be in the parallel state, the spin-up electron will pass through the structure with minimal scattering. The spin-down electron will undergo significantly more scattering in both layers and thus have a higher resistance as seen in the equivalent circuit model (Fig. 7.1b). The parallel state has two paths: one with two low resistances in series and one with two high resistances in series. If the distribution of conducting electron spins is equal in spin-up and spin-down states, the circuit in the parallel state has an overall lower resistance than that in the antiparallel state.

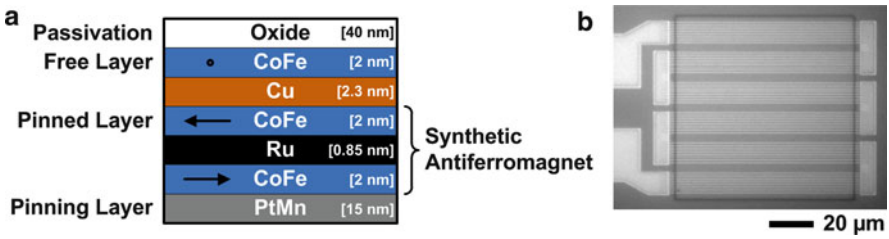

Fig. 7.2 (**a**) Representative structure of GMR SV film stack annotated with thicknesses. (**b**) Optical microscopy image of fabricated serpentine GMR SV

One drawback of the basic multilayer GMR film stack is the high magnetic field needed to fully switch the magnetization from the parallel to the antiparallel state (up to 2,000 Oe), which tends to cause the sensors to have poor low-field sensitivity [4], limiting their utility as biosensors. GMR spin-valves (GMR SV) overcome this drawback by introducing a synthetic antiferromagnet to the film stack. This antiferromagnet formed by the CoFe/Ru/CoFe structure pins the magnetization with exchange coupling. The other ferromagnetic layer, called the free layer, rotates freely with the applied magnetic field. A pinning layer, typically PtMn or IrMn, defines the magnetization of the synthetic antiferromagnetic and is also used to direct the microstructural texture of the subsequent thin films. As can be seen in Fig. 7.2, GMR SV sensors are elaborately engineered film stacks, typically only a few tens of nanometers thick, passivated with an ultrathin oxide [5].

The transfer curve of a GMR SV sensor is shown in Fig. 7.3a. The sensor adopted in this work has a minimum resistance of $2,190\Omega$ in the parallel state and a maximum resistance of $2,465\Omega$ in the antiparallel state, corresponding to 12 % MR ratio. The sensitivity of the sensor was calculated by differentiating the transfer curve (Fig. 7.3b). The sensor is most sensitive when no field is applied, tapering off as the field strength is increased. The saturation field is only 200 Oe, rendering GMR SV excellent low-field sensors.

The quest for higher MR ratios has led researchers to more exotic materials and even more elaborate film stacks. However, possibly the simplest way to increase the MR ratio is by changing the mode of operation. The original devices passed current vertically through the device as depicted in Fig. 7.1, referred to as the current-perpendicular-to-plane (CPP) mode of operation. The CPP mode of operation has a limited MR ratio because the electrons only pass through the ferromagnetic layers once and have limited opportunities to undergo spin-dependent scattering. In contrast is the current-in-plane (CIP) mode where the current flows parallel to the Cu layer and, given that the length of the sensor is significantly longer than the thickness, has many more opportunities to scatter. Figure 7.2b is an image of a device operated in CIP mode where each segment of the sensor is very long (90 μm). Typically GMR SV sensors often exhibit a 10–15 % MR ratio at room temperature.

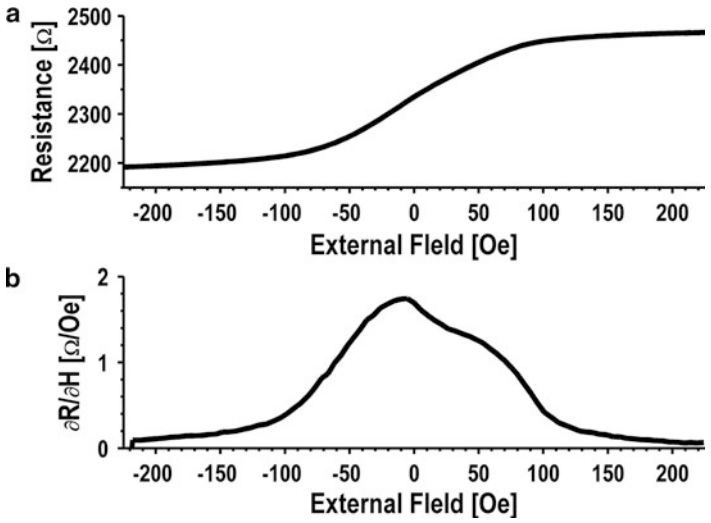

Fig. 7.3 GMR SV characterization: (**a**) transfer curve of magnetic field versus resistance; (**b**) sensitivity curve

The lower-field sensitivity of GMR SV sensors made them very attractive for many sensor applications, such as the read head in hard disk drives, current sensing, earth field sensing, and biosensing. GMR SV sensors replaced the inductive read heads in hard disk drives in the late 1990s and were key in enabling to the rapid increase in areal density and larger hard drives [6]. These GMR SV sensors have since been replaced by magnetic tunnel junction (MTJ) sensors, which exhibit even higher MR ratios. MTJs rely on an entirely different quantum mechanical effect known as tunneling magnetoresistance (TMR). Structurally the devices look very similar to a GMR SV, but the conductive Cu layer is replaced with an insulator. The orientation between the pinned layer and the free layer changes the probability that electrons can tunnel through the oxide, thus modulating the conductivity of the device. The MR ratio of these devices is often 100 % or more with the current record at 604 % at room temperature and 1,144 % at 5 K [7]. Presently, the main issue limiting the adoption of MTJs as biosensors is that with the large area of the devices, a single pin-hole defect renders the device unusable.

Despite the differences in the origin of the magnetoresistance, all magnetoresistive biosensors can be made to operate in a similar fashion. A magnetic immunoassay tethers MNP tags to the surface of the sensor. The underlying magnetically responsive biosensor detects the stray field from the MNP tags through a change in resistance. Since the stray field of the MNP tags falls off rapidly as the distance between the sensor and the tags increases, the magnetoresistive sensors can be referred to as proximity-based sensors.

7.3 Magnetic Nanoparticle Tags

Magnetic particles are commonly used in a variety of different applications such as cell sorting, magnetic resonance imaging, data storage, environmental remediation, and other applications. Here, we focus on using MNPs as tags for proteomic analysis in biomedicine. In this section, the MNP design requirements for applications to magnetically responsive nanosensors are discussed. The ideal design parameters, however, are often in conflict, thus requiring optimization choices to be made. For example, the highest signal per particle would originate from relatively large magnetic particles (on the order of 1 μm or larger). Larger particles, however, are not necessarily optimal because they tend to settle as they lack colloidal stability and they have significantly slower diffusion times. Therefore, in selecting the ideal MNP tag, competing factors must be considered and trade-offs must be made.

7.3.1 Superparamagnetism

An important design requirement for this technology is that the magnetic tags must not aggregate, chain, or precipitate during the course of any given experiment. Thus, the particles used in magnetically responsive and proximity-based detection systems ideally should be superparamagnetic, where the volume of the ferromagnetic core is so small that thermal energy alone is large enough to cause the magnetic moment of the cores to fluctuate rapidly. The average magnetic moment over time of any given superparamagnetic core is therefore zero, resulting in zero remnant moment. However, when an external magnetic field is applied, the nanoparticles magnetize with a much greater magnetic susceptibility than paramagnetic materials.

More specifically, a superparamagnetic material is a magnetic material of such small size that at temperatures below the blocking temperature, it behaves like a paramagnetic material. As the size of these superparamagnetic particles increase, they lose their superparamagnetic nature and become ferromagnetic. This limit is known as the "superparamagnetic radius." This superparamagnetic radius can be calculated by the following equation:

$$P = v_0 e\left(-\frac{\Delta f V}{k_B T}\right) \tag{7.2}$$

where P is the probability per unit time that the magnetization will change direction, v_0 is the attempt frequency ($\sim 10^9\,\mathrm{s}^{-1}$), $\Delta f V$ is the free-energy barrier that the particle must overcome in order for the moment of the particle to switch directions, k_B is Boltzmann's constant, and T is the temperature. Therefore, if iron oxide nanoparticles, for example, are to be utilized in our assay, it is favorable to use them at sizes smaller than the critical size (so they remain in the superparamagnetic regime). The challenge in using such small MNPs, however, is that as the size of the

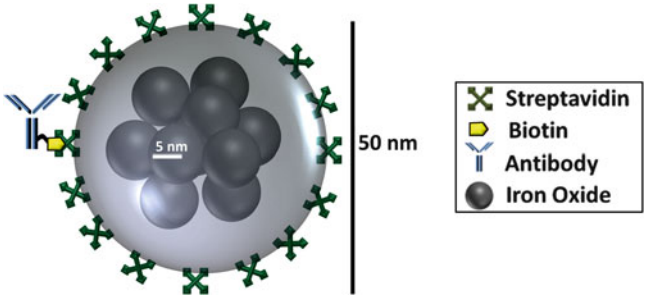

Fig. 7.4 Schematic representation of a magnetic nanoparticle (MNP) labeled with antibody drawn to scale. The magnetic tag is comprised of a dozen iron oxide cores embedded in a dextran polymer and then functionalized with antibody or receptor [8]

nanoparticle decreases, the magnetic moment decreases as well, causing the signal per particle to decrease.

The solution to this problem is to cluster many MNPs into a dextran polymer (Fig. 7.4). In this way, the MNPs are physically isolated, allowing them to remain superparamagnetic, while the overall magnetic content per magnetic tag is relatively large due to the multiplicity of cores in each cluster.

7.3.2 Application of Magnetic Nanoparticles for Magnetic Biosensing

Recent work has adapted magnetically responsive sensors for the detection of biological species in solution by implementing a traditional sandwich assay directly on these magnetically responsive nanosensors and utilizing superparamagnetic nanoparticles as tags. If a magnetic particle similar to the one described above is introduced to label the biomolecule of interest, magnetically responsive sensors are capable of highly sensitive protein and oligonucleotide detection [2, 9–12].

Among the more commonly used MNP tags in GMR biosensors are those comprised of clusters of monodisperse Fe_2O_3, superparamagnetic particles each with a 10 nm diameter embedded in a dextran polymer and functionalized with streptavidin (Fig. 7.4), as determined by TEM analysis [13]. The entire nanoparticle averages 46 ± 13 nm in diameter (measured by number-weighted dynamic light scattering). Based on the Stokes-Einstein relation, these particles have a translational diffusion coefficient of approximately $8.56 \times 10^{-12}\,m^2\,s^{-1}$. The MNPs have a reported zeta potential of -11 mV [14]. These particles are superparamagnetic and colloidally stable, so they do not aggregate or precipitate during the reaction. Therefore, a major advantage of using these tags is that the magnetically responsive sensors detect the exact same signal before and after washing (Fig. 7.5). This means that it is equally valid to read the sensor signal prior to a final wash that removes unreacted

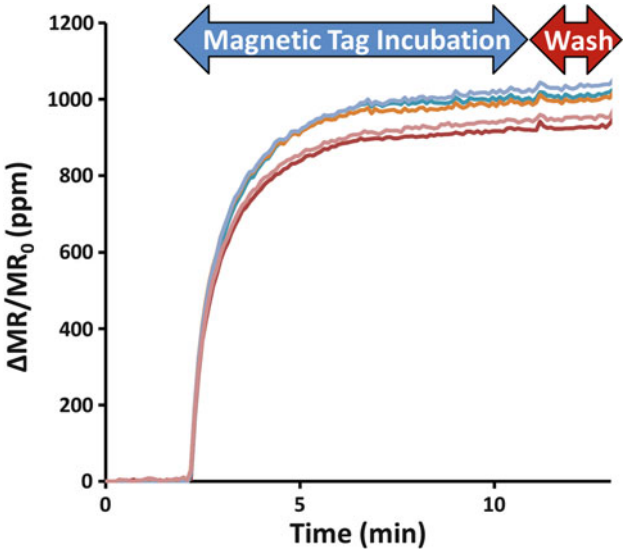

Fig. 7.5 Demonstration of negligible nonspecific binding of MNPs to the sensor surface. Shown above are binding curves for carcinoembryonic antigen (CEA) using a traditional sandwich assay. In this format, the final washing step (of three washing steps in total) is used to remove the unbound magnetic nanotags. However, as a direct result of the minimal nonspecific binding, the signal remains unchanged after the final washing step, permitting removal of the final washing step without distorting the final signal [15]

MNPs. Importantly, the magnetically responsive sensors operate as proximity-based detectors of the dipole fields from the magnetic tags. Therefore, unbound MNP tags contribute negligible signal in the absence of binding, rendering this unique nanosensor-MNP system ideal for real-time kinetic analysis [8].

It is apparent from plotting the magnetic moment per particle versus the applied external magnetic field that there is very minimal coercivity in these particles confirming their superparamagnetic nature (Fig. 7.6). In our experience, these MNPs have performed the best in terms of the kinetics of binding to detection antibody, minimal nonspecific binding, and high reproducibility.

In summary, choosing the magnetic label is a vital aspect to any magnetic biosensor where important design trade-offs must be made. On the one hand, larger, micron-sized magnetic particles are desirable as they will generate a high signal per particle. Larger particles, however, are kinetically unfavorable since detection requires diffusion of the magnetic tags to the surface-immobilized detection antibody. Furthermore, larger particles are undesirable because nonspecific binding events of micron-sized particles will have a much greater effect on the overall signal than will a nonspecific binding event of a nanoparticle. Accordingly, the optimal balance is to use MNPs that are comprised of a cluster of small superparamagnetic particles imbedded in a dextran polymer. This configuration will increase the magnetic content of each particle while remaining superparamagnetic.

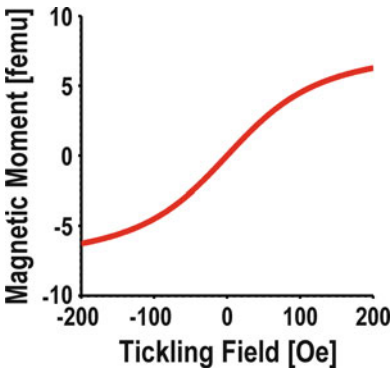

Fig. 7.6 Normalized plot of the magnetic moment per particle versus the applied external magnetic field

7.4 Protein Detection Assay Using Magnetic Nanoparticles

7.4.1 Standard Protein Detection Assay

Biomarkers can be detected either by their accumulation at a stationary binding site over a sensor surface or by the binding of biomarkers to tags in a solution inducing aggregation of the magnetic tags. For the GMR nanosensors discussed in this chapter, the former will be described. For NMR-based biosensors discussed in Chaps. 9 and 10, the latter method of protein detection will be described. One of the most effective and specific methods of detecting proteins on a sensor surface, like a GMR nanosensor, is by means of a "sandwich assay." Typically known for its use in the enzyme-linked immunosorbent (ELISA), the sandwich assay involves the formation of a three-layered structure where two antibodies (or aptamers, diabodies, Fab fragments, etc.) form a sandwich around a protein (also called the "analyte") of interest (Fig. 7.7a). One of the antibodies, generally referred to as the "capture antibody," is directly immobilized on the sensor surface. In order to make the sandwich assay highly specific, a monoclonal capture antibody is traditionally used. A solution of monoclonal antibodies means that every antibody in the solution has the exact same Fab region and therefore will bind to only one epitope on one protein. The capture antibody makes up the foundation of the sandwich assay and serves to selectively immobilize a specific protein of interest directly over the sensor surface.

The second antibody, known as the detection antibody, is delivered in solution and binds to a second epitope on the captured protein of interest. The detection antibody is typically polyclonal and pre-modified with a reactive chemistry, enabling facile attachment of the detection antibody to the tag of interest. A polyclonal antibody solution is one in which all the antibodies react with the same protein; however, they may bind to different epitopes on that protein with varying affinities. Therefore, the Fab region is not uniform across all the antibodies in a polyclonal solution but recognizes different regions of the same protein. Typically the detection

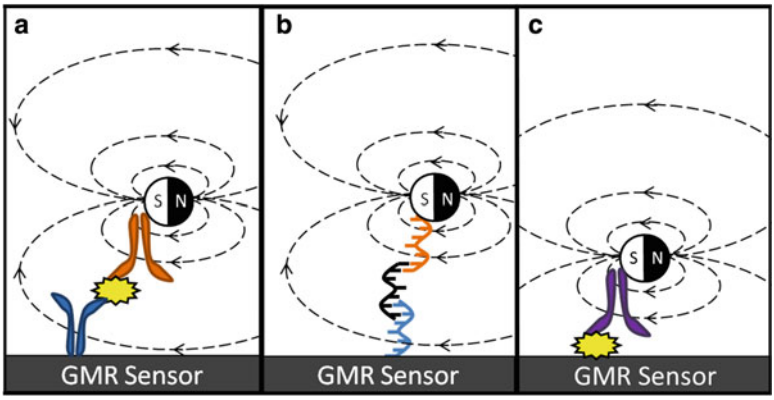

Fig. 7.7 (**a**) General schematic of a protein sandwich assay built from bottom to top with the capture antibody, analyte, and detection antibody attached to a magnetic nanotag. (**b**) General schematic of the DNA sandwich assay with the capture DNA, target DNA (shown in *dark black*), and detection DNA shown, built from bottom to top and attached to a magnetic nanotag. (**c**) Schematic of reverse-phase protein assay with target protein spotted directly on the GMR sensor surface and bound detection antibody with attached magnetic nanotag

antibody is modified with biotin, and the tag is modified with streptavidin since the biotin-streptavidin interaction is one of the strongest non-covalent receptor-ligand interactions in biochemistry (association constant, $K_a \approx 10^{14}$–$10^{15}M^{-1}$). In the ELISA, the tag of interest is typically colorimetric or fluorescent. However, when using magnetically responsive biosensors, the tag of interest is magnetic. Therefore, the more protein that is present in the system, the more detection antibodies bind and the more magnetic tags bind. As the number of magnetic tags increases over the sensor, the MR in the underlying magnetically responsive sensor changes proportionally, producing larger signals. In this way, quantitative protein detection is possible with this assay. Similar to a protein sandwich assay, it is also possible to form a DNA or RNA sandwich structure by utilizing a capture oligonucleotide sequence and biotinylated detection oligonucleotide sequence for highly sensitive nucleic acid detection (Fig. 7.7b).

A "reverse-phase" assay can be used to detect proteins of interest in many patients' blood samples simultaneously by reorganizing the traditional sandwich assay (Fig. 7.7c). In the reverse-phase assay, instead of functionalizing a capture antibody onto the sensor surface, patient samples containing proteins of interest such as cell lysates are immobilized directly onto the GMR sensor array. Then, a solution containing detection antibodies complementary to the protein of interest is introduced and will bind to the immobilized protein of interest over the GMR sensor. Since the detection antibody is biotinylated, it can then bind to magnetic nanotags coated with streptavidin in the same way as the detection antibody and magnetic nanotag interaction in the traditional sandwich assay. In addition, if one separates

the protein of interest from the sample prior to sensor immobilization using protein purification techniques, it is possible to increase capture protein density, thereby maximizing signal.

7.4.2 Wash-Free Protein Detection Assay for POC

With magnetic biosensors, the traditional sandwich assay described above can be redesigned to leverage the proximity-based detection capabilities and unique magnetic properties of a magnetically responsive biosensor system. The GMR nanosensors, for example, can be built with an ultrathin passivation layer. As discussed above, these GMR sensors are proximity-based sensors, and therefore, only magnetic nanotags within ∼150 nm of the surface are detected [5]. Because the magnetic nanotags typically employed are on the order of 50 nm in diameter and colloidally stable, they do not settle or precipitate on the sensor surface, contributing negligible signal in the absence of the target protein or detection antibody. Only in the presence of both the biomolecule of interest and detection antibody will the magnetic nanotags congregate over the appropriate sensor in close enough proximity and in high enough density for the GMR sensor to experience a measurable magnetoresistance change. This is a significant advantage over the vast majority of protein detection platforms in which the excess/unreacted tags must be washed away prior to detection, preventing their ability to utilize a wash-free detection method. As a result, while performing a traditional sandwich assay requires washing steps to remove excess antibodies or nanotags, with magnetic nanotechnology, the signal remains unchanged with a final wash step. Accordingly, the protein content can be determined in the assay without implementing washing (Fig. 7.5). Thus, because this assay obviates the need for washing steps, it offers a faster, simpler testing process that untrained users can easily perform in point-of-care settings.

By taking advantage of the "autoassembly" nature of this assay, only minimal human intervention is required to run a test, removing the dependence on the end user to have prior laboratory training. Moreover, the assay can be run in an open-well format, removing the need for complex microfluidic plumbing or external pneumatic pressure controllers. The wash-free assay entails only three steps: (1) The operator places the biological sample into the reaction well which is equipped with an array of GMR sensors pre-functionalized with a panel of antibodies against predetermined proteins of interest. As the sample incubates in the well, the proteins of interest are captured by the immobilized antibodies directly over individually addressable GMR sensors. (2) The user adds a solution of magnetic nanotags labeled with streptavidin. At this point, no detectable reaction takes place because no biotin is present in the reaction well (Fig. 7.8a). (3) Finally, detection antibodies labeled with biotin are introduced. These detection antibodies subsequently link the magnetic nanotags to the captured analyte, thus inducing a measurable signal in the underlying GMR

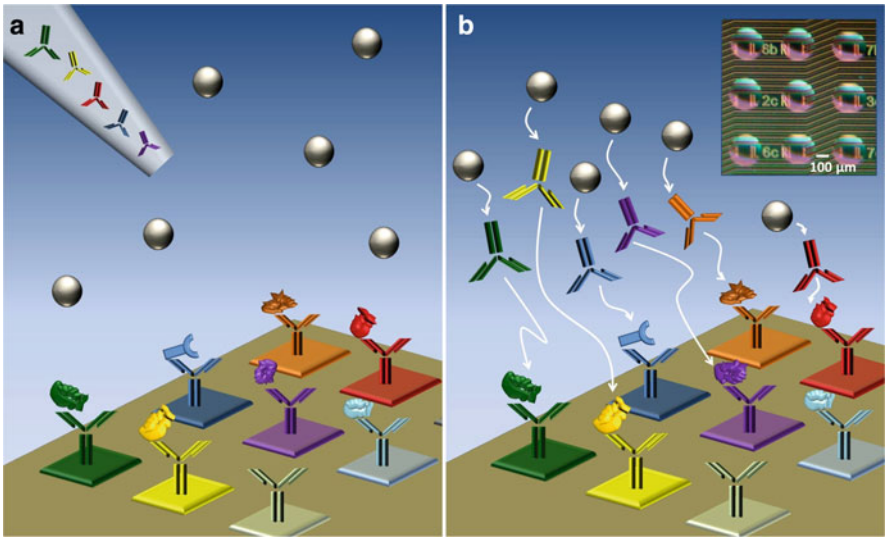

Fig. 7.8 Schematic representation of the autoassembly immunoassay where each square represents a unique GMR nanosensor in the array. (**a**) After immobilizing unique capture antibodies over individually addressable sensors, and incubating with the protein of interest, the magnetic nanotags are added in solution above the sensor. Since there is no chemistry to link the magnetic nanotags to the captured antigen, no signal is detected by the underlying sensor. (**b**) Once the detection antibody in solution is added, the detection antibody which is labeled with biotin is capable of linking the streptavidin-labeled magnetic nanotag to the captured analyte. In the presence of captured analyte, the magnetic nanotags will congregate over the corresponding GMR sensors in high enough concentration to be detected. *Insert*: optical microscopy of a section of the array of nanosensors. Each *square* in the array is one sensor and each *circle* is a nanoliter droplet of capture antibody uniquely functionalized over the sensor surface [15]

sensor (Fig. 7.8b). Each sensor in the array is monitored in real-time, providing multiplex protein detection (Fig. 7.9). Piezoelectric robotic spotter technology is used to spot 350 picoliter droplets of capture antibody onto individually addressable GMR nanosensors for high-density protein detection (Fig. 7.8b insert).

7.4.3 Microfluidic Integration of Magnetic Biosensors for POC

Among the advantages of magnetic nanosensors is that they can be fabricated into high-density arrays with minimal increase in cost or size of the overall chip. This allows for highly multiplex protein detection in a single reaction well. While there are significant advantages to open-well protein detection systems, there are several limitations as well. An open-well format is limited to running only one sample per chip. For high-throughput analysis with fewer than 5 biomarkers of interest

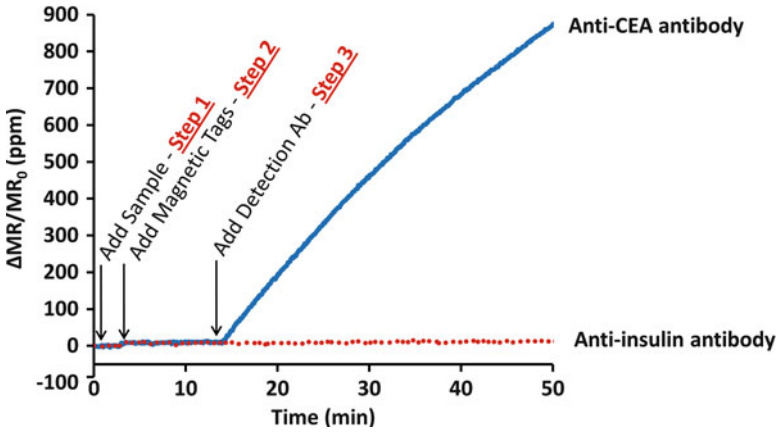

Fig. 7.9 Real-time monitoring of sensors during autoassembly immunoassay. Addition of the sample and magnetic nanotags contribute negligible signal (upon addition of the magnetic nanotags, there is a very small signal rise due to detection of magnetic nanotags in solution above the sensor). However, once the detection antibody is introduced, the magnetic nanotags are clearly measurable on sensors functionalized with the appropriate capture antibody and antigen. The negative control sensors, coated with anti-insulin antibody, remain flat, indicating negligible nonspecific binding. The y-axis units are the change in magnetoresistance normalized to the initial magnetoresistance presented in parts per million (ppm)

per sample, it is wasteful and underutilized to have on the order of 100 sensors per nanosensor array investigate only five biomarkers. It would be more efficient if the high-density sensor array could be subdivided where several patient samples could be run simultaneously on a single chip using parallel microfluidic channels. In addition, with cross-reactive antibodies, reagents can be separated into their own reaction chambers when implementing microfluidic integration in order to minimize this phenomenon. Further, the use of microfluidics can be optimal for handling biological samples when only very small sample volumes are available. Fortunately, microfluidic chip integration is highly compatible with magnetic nanosensor arrays (Fig. 7.10). In this very basic microfluidic chip, each microfluidic channel contains eight sensors for up to 8-plex protein detection on any given sample in any given channel. This will yield eightfold more tests per hour and amortize the chip cost over multiple samples.

The microfluidic chips are fabricated using standard soft lithography techniques. Polydimethylsiloxane (PDMS) is cast onto an SU8-based mold. The PDMS is then cured and peeled from the mold. The thickness of the mold is used to form the fluidic channels. External connections are then punched into the inlets and outlets of the PDMS blocks. The final microfluidic chip design is comprised of 200 − μm-wide channels that are each 20 μm high and the channel pitch is 400 μm. For more details on microfluidic biosensors, please refer to Chap. 2.

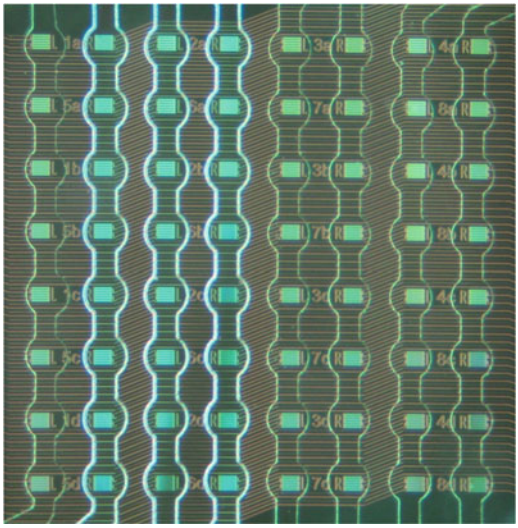

Fig. 7.10 Microfluidic chip comprising eight parallel microfluidic channels for high-throughput sample analysis

7.5 Miniaturization of Desktop Biostation

In order to facilitate effective deployment in the field by nontechnical users, it is important that the wash-free assay be integrated into an ultraportable and battery-powered detection module [16]. This capability should obviate the need for a constant supply of electricity or a designated laboratory. Since the form factor of GMR nanosensors is very small, dictated only by lithography used in their fabrication, by miniaturizing the electronic components, it is possible to replace a laboratory full of equipment with a handheld and battery-powered device (Fig. 7.11). No lasers or expensive charge-coupled device (CCD) cameras are required for the platform, which uniquely positions GMR-based biosensors for ultraportable, POC applications.

The detection platform has been designed to have two components: a reusable handheld detection module the size of a handheld calculator (Fig. 7.12a) and a disposable detection stick (Fig. 7.12b). The handheld detection module consists of two boards. First, the data acquisition board (DAQ) has both analog and digital subcircuits. The analog circuits are comprised of the excitation signal generation, the field signal generation, and the front end. The front end for the sensor is a classical Wheatstone bridge with a high-gain instrument amplifier. Also contained on the DAQ board is the microprocessor which does the digital signal processing (DSP) and handles all of the user interactions. The other board in the detection module is the coil board which contains a power amplifier and a planar electromagnet used to generate the magnetic field to modulate the sensors. The disposable stick, which is the second component of the overall detection platform, contains no electronics, just the GMR nanosensor array with 8 individually addressable sensors

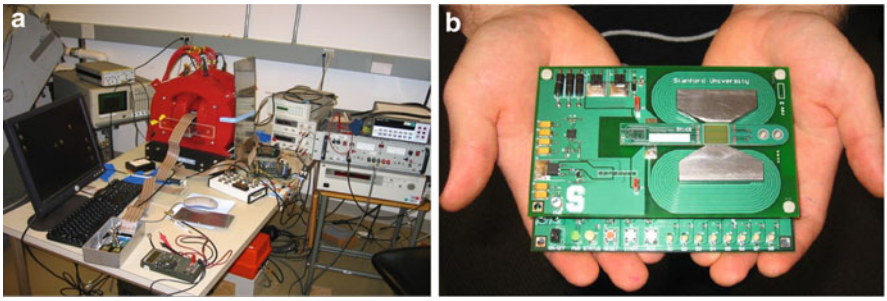

Fig. 7.11 Miniaturization of the original biostation into a handheld, battery-powered device. Demonstration of miniaturization from (**a**) the initial laboratory test station which occupied an entire room into (**b**) handheld point-of-care diagnostic device. All components of the laboratory setup have been miniaturized and incorporated into an ultraportable platform [17]

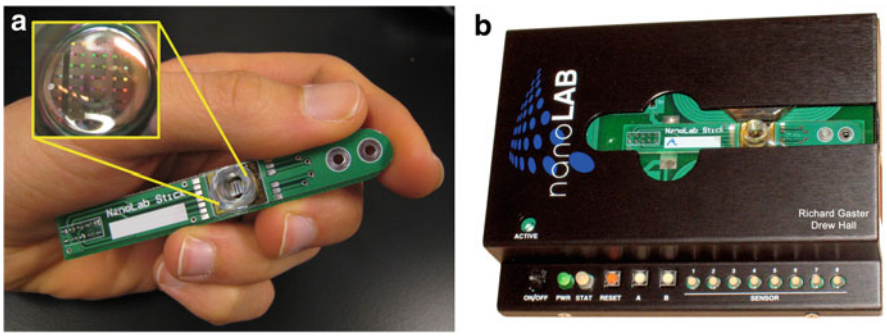

Fig. 7.12 (**a**) Photograph of the disposable stick and reaction well in which the assay is run. *Insert*: Inside the reaction well is an array of GMR sensors capable of simultaneously monitoring multiple different proteins in a 20–50 − μL sample. (**b**) Image of the handheld device with case and test stick

for multiplex detection, mounted on a printed circuit board (PCB). The disposable stick also has an open well surrounding the GMR nanosensor array where the wash-free protein detection assay is run. The disposable stick can be pre-functionalized with capture antibodies to detect biomarkers for cardiovascular disease, cancer, influenza, HIV, and a variety of other chronic and infectious diseases.

One of the largest and most difficult elements to miniaturize in the research grade biostation was the Helmholtz electromagnet. This large component alone weighs over 100 kg and when coupled with the associated power amplifier, consumes over a hundred watts of power drawn from a wall outlet. In the typical research setting (Fig. 7.11a), the size and cost of a magnetic test station are not critical factors because the main goal is often to maximize the sensitivity, linear dynamic range, and throughput.

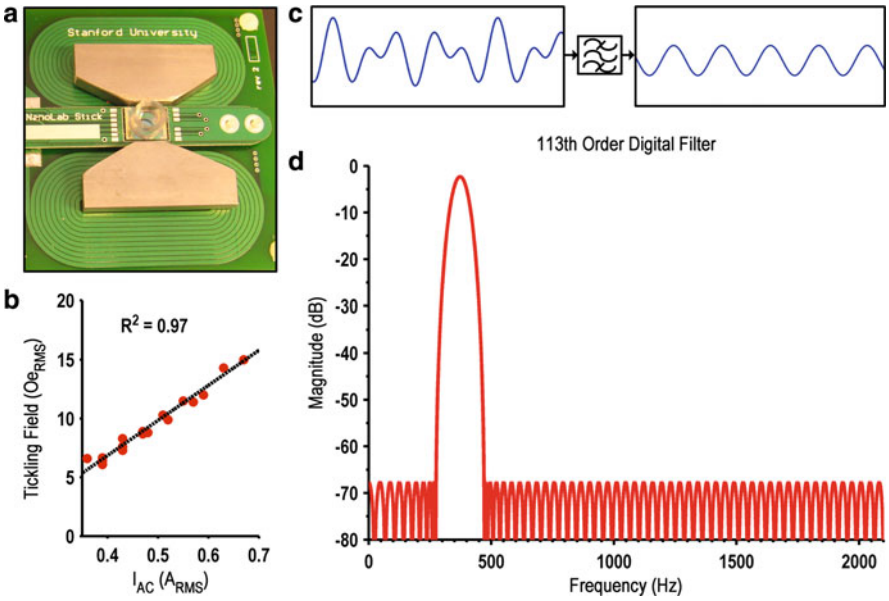

Fig. 7.13 (**a**) Photograph of planar electromagnet and flux guides. (**b**) Measured magnetic field versus current applied to the electromagnet. (**c**) Time domain signal from the GMR nanosensors before and after applying the digital filter. (**d**) Transfer function of the 113th order digital finite impulse response (FIR) filter [17]

In contrast, reducing the form factor and power consumption to create a handheld, ultraportable device is essential for POC application, but posed several engineering challenges. To accomplish this miniaturization, a planar electromagnet was designed using 1.27-mm (50 mil) traces on a four-layer PCB (Fig. 7.13a). The orientation of the current flowing through the coil alternates between clockwise and counterclockwise to avoid the need for any crossover traces that would reduce the number of available routing layers. The magnetic field is generated out of the plane (perpendicular to the PCB) and reoriented by soft magnetic flux guides manufactured out of cold rolled steel. The flux guides concentrate the field over a smaller region, acting as a form of passive amplification, and are used as heat sinks for the electromagnet. In addition to the flux guides above the coil, there are flux guides below the coil to close the flux loop and increase the efficiency. Due to the off-axis nature and the use of magnetic flux guides, analytical models are not tractable for design. Instead, finite element modeling (FEM) is needed to determine the required number of turns (11 turns per layer) and current, which includes both field strength and frequency. The miniature electromagnet is driven by a custom-designed class-A power amplifier. Figure 7.13b illustrates the relationship between the current through the electromagnet and the measured field across the GMR SV. Power consumption was minimized by cycling the power amplifier and electromagnet when they are not being used.

Currently, proteomics in clinical (not POC) settings utilize fluorescent detection based on the ELISA, which report detection limits on the order of 1 pM with 2 orders of linear dynamic range. The wash-free assay presented here has a similar dynamic range but achieves over an order of magnitude higher sensitivity in a fraction of the time. The higher sensitivity is primarily attributable to using MNP tags rather than fluorescent labeling. With the magnetic nanotechnology described in this chapter, detection down to 50 fM in a 25 μL sample has been demonstrated [17]. While the sensitivity needs for POC settings is generally less stringent, having higher sensitivity allows for a shorter assay time, leading to faster diagnostic times. The higher sensitivity of this technology may also facilitate the earlier diagnosis of disease.

The MNP tags require an external magnetic field to induce a magnetic moment, and the sensors require the magnetic field to modulate the sensor response to a higher frequency. The optimal magnetic field for this particular combination of sensor and MNP has been shown previously to be 25 Oe [18]. Because the optimum is fairly shallow, this allows the field to be reduced without a significant loss in sensitivity. At a magnetic field of 15 Oe (60 % of the optimum), the signal per MNP decreases by only 20 %. With this small reduction in sensitivity, the power consumption can be significantly reduced.

GMR spin-valves typically exhibit high flicker noise (also known as $1/F$ noise because it is inversely proportional to frequency). To increase the signal-to-noise ratio (SNR) and improve the detection capability of the device, the signal from the MNP tags is modulated away from the low-frequency noise to a higher frequency [19]. To recover this signal, the microprocessor digitizes the response from the GMR nanosensors and performs the filtering and demodulation. Figure 7.13c, d illustrates this process with the incoming modulated signal and the clean output signal after a 113th order digital filter has been applied. A minimalistic version of the computationally intensive signal processing algorithms used in our desktop station was implemented due to the limited computational power of the microprocessor [20]. With the integration of a power source, signal processing, and display functionality into the handheld detection module, no additional components are required to run and measure an assay, allowing it to truly be a POC testing device.

A fundamental element of the handheld device is a microchip microprocessor (dsPIC30F6012a) which runs at 80 MHz (20 MIPS). The microprocessor has an integrated 12-bit analog to digital converter used to digitize the signals from the sensors. Furthermore, the microprocessor communicates to the direct digital synthesizer chips via an integrated SPI bus. However, the primary reason for choosing a high-end microprocessor is for the heavy DSP algorithms that it performs. To extract the single tone from the spectrum with the double modulation scheme, the 113 tap digital FIR bandpass filter is applied to the incoming samples. The tap count was chosen after all of the code had been written such that it filled the remaining memory of the microprocessor to minimize the noise bandwidth of the extracted tone. The root mean square value of the filter output is proportional to the magnetoresistance of the sensor and is saved to an internal buffer. The sensors are scanned in a round robin fashion, rotating from sensor 1 through sensor 8. For each

sensor, the signal is acquired for 200 ms and the subsequent analysis takes 800 ms. While the signal processing could be overlapped with the data acquisition or applied in real-time, the tasks are undertaken sequentially to simplify the timing between the acquisition and the processing steps. This signal acquisition and processing is repeated throughout the duration of the test.

In POC settings, it is not practical to perform sample preparation prior to running the diagnostic test. Accordingly, the platform must have reproducible detection despite differences in the sample fluid (buccal swab, serum, urine, cell lysates, etc.), pH, and temperature. Fortunately, GMR spin-valve sensors have been reported to be insensitive to different sample matrices, rendering the platform highly generalizable to a diversity of biologically relevant samples and removing the need for any complex sample preparation [21]. This subtle requirement is often overlooked or ignored when discussing POC diagnostics, but in fact is critical to the utility of such a diagnostic device in real-world settings.

7.6 POC Detection Results via GMR Biosensor Arrays

The user interface of the detection module has been designed to provide both a rapid readout and a user-friendly, easy-to-comprehend display. The microprocessor monitors the real-time binding events and predicts the saturation signal based on the initial binding trajectory. Monitoring the binding trajectory in real-time significantly reduces the assay time and produces a more reliable final readout than taking a single-point measurement at an arbitrary time prior to signal saturation. Figure 7.14a shows the binding curves of various concentrations of human immunodeficiency virus (HIV) p24 protein ranging from 100 ng/mL down to 32 pg/mL. We used these binding trajectories to train the microprocessor for future experiments. The assay runs for 15 min to allow sufficient time for differentiable signals to emerge while still providing rapid results for POC utility.

Each disposable stick, which is inserted into the detection module, is equipped with eight sensors allowing for up to 8-plex protein detection simultaneously in a single assay and permitting entire panels of markers to be monitored in real-time. The signals detected by each sensor on the stick can be displayed to the user via colored light-emitting diodes (LEDs) on the detection module. The microprocessor is preprogrammed with tables that contain calibration curves for each target protein as well as for the corresponding concentration thresholds (undetectable, low, medium, and high) which are predetermined by physicians according to clinically relevant therapy regimens (Fig. 7.14b). As the assay runs, the colored LEDs dynamically change and thereby present the results in real-time to the end user. The display of the device can alternatively be equipped with a quantitative digital readout, but the LED color reporting system shown here suffices to indicate relative levels of protein content for untrained users. After a 15 min incubation period, the predicted signal at saturation is compared with threshold values, and the microprocessor selects the appropriate indicative color for each LED. For example, when a 10 ng/mL of p24 capsid protein was tested on the handheld device, a signal of 39 ppm was measured

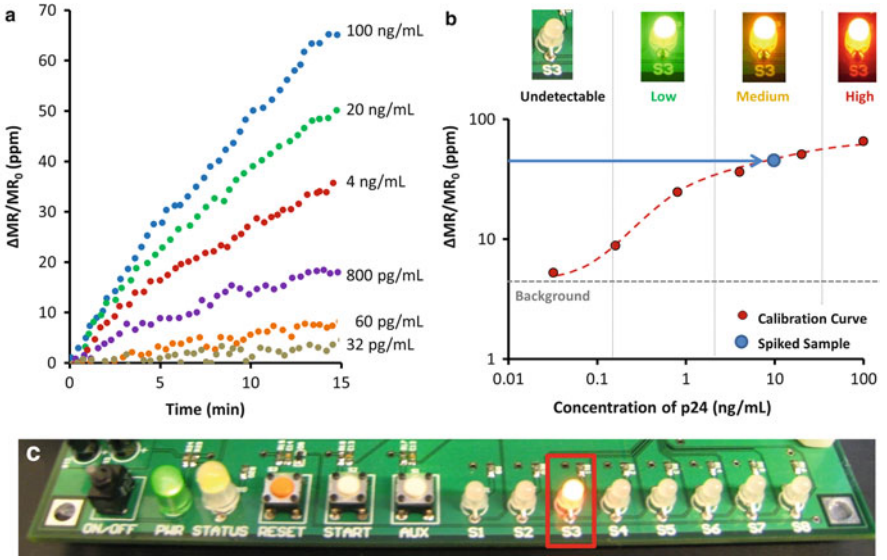

Fig. 7.14 Detection characteristics and readout of the handheld magnetic biosensor. (**a**) Real-time binding curves of diluted HIV p24 protein at concentrations ranging from 100 ng/mL to 32 pg/mL. The sensors, functionalized with bovine serum albumin (BSA) as a negative control, gave minimal signal indicating negligible nonspecific binding of the wash-free assay. (**b**) Calibration curves for each marker of interest were generated after 15 min of incubation time. The final curve is subsequently divided into four predetermined concentration ranges and will be presented via color coded LEDs to the end user. If the signal is undetectable, the indicator light will not be lit. If the signal is low, medium, or high, then the light indicator will display green, orange, or red light, respectively. (**c**) To demonstrate the specificity and readout of the device, we functionalized each of the eight sensors with a different capture antibody. For example, sensor S3 was functionalized with anti-p24 antibody. When 10 ng/mL of p24 antigen was spiked into the reaction well, only sensor S3 lit up in the medium concentration regime [17]

and the LED for sensor 3 (on the device labeled S3) turned orange, indicating a moderate level of protein content (Fig. 7.14b and c). As appropriate, all the other sensors, functionalized with noncomplementary antibodies, registered no signal. Similar experiments have been demonstrated with detection of hepatitis C virus (HCV) capsid protein [22], presented in Fig. 7.15. The combination of a rapid, wash-free assay and user-friendly display system can help facilitate the rapid adoption of this platform in both urban centers as well as remote field settings.

Another important consideration for POC applications is that the platform should be cost-effective. The total cost of each disposable stick (including the antibodies, magnetic tags, sensors, and assembly) in high volume is less than $3.50 (Table 7.1), which means that this diagnostic tool is sufficiently cost-effective to be used in both developing and developed nations. Furthermore, we believe the cost could be substantially reduced to less than $1 with slight changes to the sensor array and by preparing the MNPs in-house.

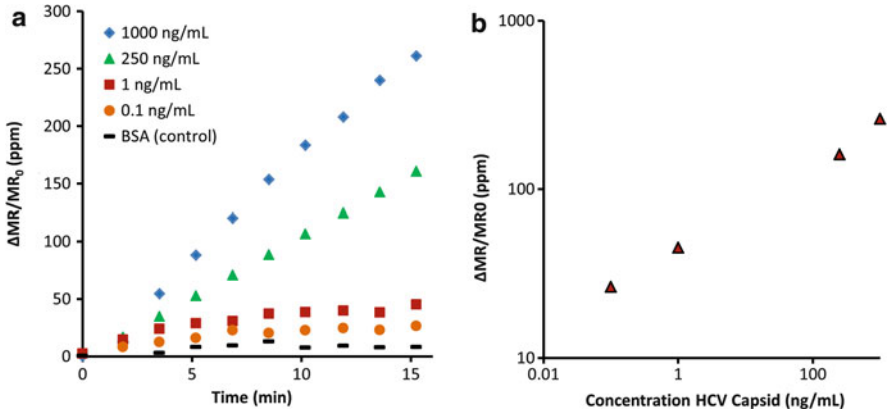

Fig. 7.15 (**a**) Real-time binding curves of diluted HCV capsid protein at concentrations ranging from 1,000 ng/mL to 100 pg/mL. The sensors, functionalized with bovine serum albumin (BSA) as a negative control, gave minimal signal indicating negligible non-specific binding of the wash-free assay. (**b**) Calibration curves for each marker of interest were generated after 15 min of incubation time on a log-log scale [17]

Table 7.1 The itemized cost of the one-time use disposable stick, including the circuit board, sensors, capture and detection antibodies for eight sensors, magnetic nanoparticles, surface chemistry, and assembly, is shown below. The volume of production is calculated for one million units per year. It is further assumed that the antibodies are robotically spotted to reduce the required volume and assembly cost

Item	Unit cost ($)
Circuit board and connector	0.34
GMR sensor die	1.00
HCV capture antibody (abcam 2583)	0.03
HCV detection antibody (abcam 58713)	0.03
Magnetic nanoparticles (Miltenyi Biotec 130-048-101)	1.88
Surface chemistry reagents	0.01
Assembly	0.20
Total	**3.49**

7.7 Conclusions

The handheld device described in this chapter has the potential to provide a significant contribution to the future of POC medical diagnostics. As the population continues to expand and societal mandates for universal healthcare grow, innovations in diagnostic testing will be required to provide timely, easily accessible, and inexpensive results. To meet this need, it is necessary to develop cost-effective, portable, and easy-to-use devices which allow individuals to conduct their own molecular diagnostic tests without the need for a centralized laboratory, laboratory technicians, clinic or emergency room visits, or in some instances visits to a physician's office.

While significant strides have been made toward developing a true POC testing device using magnetic nanotechnology [23–25], systems designed prior to this work have relied on an external power source and an external PDA (either a pocket PC or a laptop) for signal processing, data logging, and display. In the work presented in this chapter, a fully integrated and cost-effective unit incorporating a built-in microprocessor and miniature electromagnet has been designed to perform all of these tasks. The handheld biomarker detection platform utilizing magnetically responsive biosensors and MNP tags has tremendous potential for POC diagnostics and personalized medicine. Throughout the development of this technology, a conscious effort was made to create a platform that is both cost-effective and power efficient for portable applications. The handheld detection module consumes an average of 3.7 W from a rechargeable battery and weighs only 0.34 kg (0.75 lbs). Moreover, the sensitivity of this handheld device and its multiplex capability are noteworthy. The protein detection limit of 50 fM and 8-plex protein detection achieved by this device are on par with or exceed many of the current desktop protein detection platforms.

With the presented magnetic nanotechnology, patients can receive accurate molecular-based diagnosis on their own in a matter of minutes. Furthermore, due to the versatility of the sensing platform, the potential applications are vast, particularly in the realm of infectious diseases. By providing disposable sticks pre-functionalized with different capture antibodies, this technology can be deployed for detection of a range of infectious diseases that pose large-scale public health risks, such as HIV, HCV, tuberculosis, *Salmonella typhi*, and toxigenic *E. coli*, as well as swine (H1N1) flu and avian (H5N1) flu. In addition, screening for enteric infections is of particular interest, as the device will enable public health officials to inspect and immediately detect contamination on-site, to aid in safeguarding food and water sources for populations worldwide. This technology has the potential to reshape the practice of medicine by providing societies in both the developed and developing world with a new medical infrastructure: one that gives individuals the tools to literally take healthcare into their own hands.

Acknowledgements This work was supported, in part, by the United States National Cancer Institute (grants 1U54CA119367, 1U54CA143907, 1U54CA151459, 1U01CA152737, 5R33CA138330, and N44CM-2009–00011), the United States National Science Foundation (grant ECCS-0801385–000), the United States Defense Advanced Research Projects Agency/Navy (grant N00014–02–1–0807), a Gates Foundation Grand Challenge Exploration Award, and the National Semiconductor Corporation. RSG acknowledges financial support from the Stanford Medical School Medical Scientist Training Program and the National Science Foundation Graduate Research Fellowship Program.

References

1. R. Kotitz, H. Matz, L. Trahms, H. Koch, W. Weitschies, T. Rheinlander, W. Semmler, and T. Bunte, SQUID based remanence measurements for immunoassays, *IEEE Transactions on Applied Superconductivity*, vol. 7, pp. 3678–3681 (1997)

2. D.R. Baselt, G.U. Lee, M. Natesan, S.W. Metzger, P.E. Sheehan,R.J. Colton, A biosensor based on magnetoresistance technology. Biosens. Bioelectron. **13**, 731–739 (1998)
3. T.G.S.M. Rijks, S.K.J. Lenczowski, R. Coehoorn, W.J.M. De Jonge, In-plane and out-of-plane anisotropic magnetoresistance in Ni_ {80} Fe_ {20} thin films. Phys. Rev. B **56**, 362 (1997)
4. J.M. Daughton, GMR applications. J. Magn. Magn. Mater., **192**, 334–342 (1999)
5. S.J. Osterfeld, H. Yu, R.S. Gaster, S. Caramuta, L. Xu, et. al, Multiplex protein assays based on real-time magnetic nanotag sensing. Proc. Natl. Acad. Sci. **105**, 20637 2008
6. C.H. Tsang, R.E. Fontana, T. Lin, D.E. Heim, B.A. Gurney, M.L. Williams, Design, fabrication, and performance of spin-valve read heads for magnetic recording applications. IBM J. Res. Develop. **42**, 103–116 (1998)
7. S. Ikeda, J. Hayakawa, Y. Ashizawa, Y.M. Lee, K. Miura, H. Hasegawa, M. Tsunoda, F. Matsukura, H. Ohno, Tunnel magnetoresistance of 604% at 300 K by suppression of Ta diffusion in CoFeB/MgO/CoFeB pseudo-spin-valves annealed at high temperature. Appl. Phys. Lett. **93**, 082508 (2008)
8. R.S. Gaster, L. Xu, S.-J. Han, R.J. Wilson, D.A. Hall, S.J. Osterfeld, H. Yu, S.X. Wang, Quantification of protein interactions and solution transport using high-density GMR sensor arrays. Nat. Nanotechnol. **6**, 314–320 (2011)
9. L. Xu, H. Yu, M.S. Akhras, S.-J. Han, S. Osterfeld, R.L. White, N. Pourmand, S.X. Wang, Giant magnetoresistive biochip for DNA detection and HPV genotyping. Biosens. Bioelectron. **24**, 99–103 (2008)
10. S.P. Mulvaney, K.M. Myers, P.E. Sheehan, L.J. Whitman, Attomolar protein detection in complex sample matrices with semi-homogeneous fluidic force discrimination assays. Biosens. Bioelectron. **24**, 1109–1115 (2009)
11. M. Koets, T. van der Wijk, J.T.W.M. van Eemeren, A. van Amerongen, M.W.J. Prins, Rapid DNA multi-analyte immunoassay on a magneto-resistance biosensor. Biosens. Bioelectron. **24**, 1893–1898 (2009)
12. D.L. Graham, H. Ferreira, J. Bernardo, P.P. Freitas, J.M.S. Cabral, Single magnetic microsphere placement and detection on-chip using current line designs with integrated spin valve sensors: Biotechnological applications. J. Appl. Phys. **91**, 7786 (2002)
13. A.L. Koh and R. Sinclair, TEM Studies of Iron Oxide nanoparticles for Cell Labeling and Magnetic Separation. *Technical Proceedings of the 2007 NSTI Nanotechnology Conference and Trade Show*, Santa Clara, CA, pp. 101–104, (2007)
14. R. De Palma, C. Liu, F. Barbagini, G. Reekmans, K. Bonroy, W. Laureyn, G. Borghs, G. Maes, Magnetic Particles as Labels in bioassays: interactions between a biotinylated gold substrate and streptavidin magnetic particles. J. Phys. Chem. C, **111**, 12227–12235 (2007)
15. R.S. Gaster, D.A. Hall, S.X. Wang, Autoassembly protein arrays for analyzing antibody cross-reactivity. Nano Lett., **11**, 3047 (2011)
16. J. Kling, Moving diagnostics from the bench to the bedside. Nat. Biotechnol. **24**, 891–893 (2006)
17. R.S. Gaster, D.A. Hall, S.X. Wang, nanoLAB: an ultraportable, handheld diagnostic laboratory for global health. Lab Chip **11**, 950–956 (2011)
18. D.A. Hall, R.S. Gaster, T. Lin, S.J. Osterfeld, S. Han, B. Murmann, S.X. Wang, GMR biosensor arrays: a system perspective. Biosens. Bioelectron. **25**, 2051–2057 (2010)
19. B.M. de Boer, J.A.H.M. Kahlman, T.P.G.H. Jansen, H. Duric, J. Veen, An integrated and sensitive detection platform for magneto-resistive biosensors. Biosens. Bioelectron. **22**, 2366–2370 (2007)
20. D.A. Hall, R.S. Gaster, S.J. Osterfeld, B. Murmann, S.X. Wang, GMR biosensor arrays: correction techniques for reproducibility and enhanced sensitivity. Biosens. Bioelectron. **25**, 2177–2181 (2010)
21. R.S. Gaster, D.A. Hall, C.H. Nielsen, S.J. Osterfeld, H. Yu, K.E. Mach, R.J. Wilson, B. Murmann, J.C. Liao, S.S. Gambhir, S.X. Wang, Matrix-insensitive protein assays push the limits of biosensors in medicine. Nat. Med. **15**, 1327–1332 (2009)
22. J. Lorenzo, A. Castro, A. Aguilera, E. Prieto, S. López-Calvo, B. Regueiro, J. Pedreira, Total HCV core antigen assay: a new marker of HCV viremia and its application during treatment of chronic hepatitis C. J. Virol. Methods **120**, 173–177 (2004)

23. R.L. Edelstein, C.R. Tamanaha, P.E. Sheehan, M.M. Miller, D.R. Baselt, L.J. Whitman, R.J. Colton, The BARC biosensor applied to the detection of biological warfare agents. Biosens. Bioelectron. **14**, 805–813 (2000)
24. N. Sun, T-J. Yoon, H. Lee, W. Andress, V. Demas, P. Prado, R. Weissleder, D. Ham, Palm NMR and one-chip NMR. *Solid-State Circuits Conference Digest of Technical Papers (ISSCC), 2010 IEEE International*, San Francisco, CA, pp. 488–489 (2010)
25. M. Piedade, L.A. Sousa, T.M. de Almeida, J. Germano, B.A. da Costa, J.M. Lemos, P.P. Freitas, H.A. Ferreira, F.A. Cardoso, A new hand-held microsystem architecture for biological analysis. *IEEE Transactions on Circuits and Systems I: Regular Papers*, vol. 53, pp. 2384–2395, (2006)